An experiment on free thermal convection of water in saturated permeable material

By R. A. WOODING

*Applied Mathematics Laboratory, Department of Scientific and Industrial Research, Wellington, New Zealand**

(*Received* 3 *September* 1957)

SUMMARY

A small-scale experimental model has been constructed for the study of steady-state slow free convection of water in saturated sand. The convection field is confined between coaxial cylinders maintained at constant temperature difference, and the upper and lower boundaries consist of planes with thermal and fluid insulation. Measurements of the temperature distribution within the convection space have been obtained for average boundary temperature differences $(T_1 - T_0)$ of (I) 18·40° A, (II) 32·70° A, and (III) 46·68° A. Theoretical temperature values predicted from perturbation theory have been fitted by least squares. The first-order estimates of $\eta/(T_1 - T_0)$, where η is the convection parameter or modified Rayleigh number, do not differ significantly from a constant value ($\pm 3\%$ S.D.) for the three given values of $T_1 - T_0$, indicating good agreement between theoretical and experimental results. First-order estimates are made also of the temperature coefficient of thermal conductivity b of the sand–water mixture, and of the coefficient of radiation loss c at the upper insulated boundary, but these estimates are less reliable. Separate determinations of $\eta/(T_1 - T_0)$, b, c by direct physical measurement are in good agreement with the least-squares estimates.

1. INTRODUCTION

In a recent paper (Wooding 1957), the equations governing slow free convection of liquid in saturated homogeneous permeable material have been solved approximately, using perturbation expansions of the dependent variables (temperature and stream function) in powers of a convection parameter η. The method is very closely related to the technique of expansion in powers of the Rayleigh number

$$R = \frac{\alpha(T_1 - T_0)gd^3}{\kappa_0 \nu_0}, \tag{1}$$

* Now at the Cavendish Laboratory, Cambridge.

which has been applied to problems of free convection in fluids (Batchelor 1954), and in fact

$$\eta = \frac{k\alpha(T_1 - T_0)gd}{(K_m/K_w)_0 \kappa_0 \nu_0} = \frac{N(\Delta/d)^2}{(K_m/K_w)_0} R. \tag{2}$$

Under non-isothermal conditions each of these parameters arises naturally when the corresponding equation of motion is reduced to dimensionless form—the Navier–Stokes equation in the case of R and the Darcy equation in the case of η. Hence η may be termed a modified Rayleigh number.

In equation (1), α is the linear coefficient of thermal volume expansion of the liquid, T_0 and T_1 are two reference temperatures on the absolute scale, g is the acceleration due to gravity, d is a representative linear dimension of the convection field, κ_0 is the thermal diffusivity of the liquid at temperature T_0, and ν_0 is the kinematic viscosity at temperature T_0. In equation (2), $(K_m/K_w)_0$ is the value at T_0 of the ratio of the thermal conductivity of the permeable solid–liquid mixture to the thermal conductivity of the liquid; Δ is a linear dimension proportional to the particle or pore size of the solid, and N is a dimensionless constant dependent upon the geometrical shape of the particles. The permeability k $(= N\Delta^2)$ is assumed to be constant.

Under given boundary conditions, the value of the convection parameter η may be estimated in several ways. For instance: (*a*) by physical measurement of the quantities involved in the definition of η (equations (1) and (2)), (*b*) by measurement of the distortion of the temperature field caused by convective flow of liquid, the observations being compared with a perturbation model of the form

$$\theta = \theta_0 + \eta\theta_1 + \eta^2\theta_2 + \ldots, \tag{3}$$

where θ is a temperature parameter and θ_0, θ_1, θ_2, ... are coefficients calculated from perturbation theory, (*c*) by measurement of the liquid flow rates at selected points of the convection field, the observations being compared with a corresponding perturbation model involving the stream function ψ. Methods (*b*) and (*c*) are applicable only over the range of small η for which perturbation theory is valid.

This paper describes the measurement of η by methods (*b*) and (*a*) respectively, the former method using an experimental model with water-saturated sand as the convection medium, while for the latter method, separate measurements of the fluid permeability and thermal conductivity of the saturated sand are obtained.

A particularly simple arrangement with cylindrical symmetry is chosen for the boundary conditions of the model. No attempt is made to use boundary conditions resembling those of a geothermal area, and, in fact, the latter task has been carried out recently by Mr John Elder in the Cavendish Laboratory, Cambridge. The present model, in addition to providing a preliminary check of the perturbation theory, serves to indicate a practical method of measuring directly the ratio $(K_m/K_w)_0 \kappa_0 \nu_0/k$ (see

equation (2)) for samples of material obtained in geothermal areas, although the effect of large-scale fissuring, which is normally present in active parts of such areas, would be neglected by the method.

To facilitate an accurate fit of the perturbation convection model to the experimental data, a refinement to the equation of energy transport, involving modification of the coefficient of thermal conductivity of the mixture, will be considered. This is the variation with temperature of the thermal conductivity of the solid–liquid mixture. The law of temperature dependence can be taken to be

$$K_m = (K_m)_0\{1 + b(T - T_0)\}, \tag{4}$$

where K_m, $(K_m)_0$ are the values of the thermal conductivity of the saturated permeable material at the temperatures T and T_0 respectively, and the constant b is the linear coefficient of thermal conductivity. As b can be assumed to be small, its effect for small temperature differences can be treated by first-order perturbation theory.

The diffusion or dispersion of heat due to percolation of the liquid about the sand grains can be expected to be a small effect, although it could become significant in cases of appreciably high fluid flow speeds about coarse solid particles. The phenomenon closely resembles Brownian motion in that a given fluid particle performs small random motions which are superimposed upon the main fluid motion $\mathbf{q}$. From the analogy with the classical theory of random flights (Rayleigh 1899, Chandrasekhar 1943), it is a simple matter to show that the magnitude D of the 'thermal dispersion coefficient' will obey the relation

$$D = O(\rho c \Delta |\mathbf{q}|), \tag{5}$$

where Δ is a typical dimension of the solid particles or of the pores, ρc is the heat capacity of the fluid, and $|\mathbf{q}|$ is the main flow speed. Then the apparent thermal conductivity of the saturated permeable material, for isotropic thermal dispersion, becomes $K_m + D$. If the dispersion effect is non-isotropic, its coefficient assumes a complicated tensor form (Chandrasekhar 1943). However, for very small Δ in comparison with the boundary dimensions, and with very slow fluid flow, as in the present experiment, it can be shown from (5) that D is negligible in comparison with K_m and the effect of dispersion can therefore be neglected.

For purposes of the experiment, it is necessary to consider briefly the influence of the dynamic boundary layer associated with each rigid boundary which is immersed in permeable solid material. Darcy-type flow solutions cannot satisfy the 'non-slip' condition at a rigid boundary, whence it becomes necessary to neglect the region of boundary layer flow. This approximation is justified when the Reynolds number of the flow is very small. Then all fluid velocities in the pore spaces are of laminar (Poiseuille) type, and the shape of each velocity profile across a pore space, or normal to a rigid boundary, is independent of the kinematic viscosity ν and of the main fluid flow rate $|\mathbf{q}|$. It follows that the typical thickness δ of the boundary layer depends on only the typical solid particle (or pore) size Δ, and that the ratio

δ/Δ is of order unity. This follows from the particular form of the Navier–Stokes equations for which the inertia terms are negligible, gradients perpendicular to the boundary are large compared with those parallel, and the pressure gradient is given by Darcy's law. If X is a coordinate measured along an impermeable rigid boundary immersed in saturated permeable material and Y is measured along the normal, one has

$$(\text{pressure gradient})/\rho = -\frac{\nu}{k}|\mathbf{q}| = \nu u_{YY},$$

where u is the X-component of the flow, and $|\mathbf{q}|$ is the speed of the main stream outside the boundary layer. Since $u_{YY} = O(|\mathbf{q}|/\delta^2)$, this gives

$$\delta = O(k^{1/2}) = O(\Delta), \tag{6}$$

from the relation $k = N\Delta^2$ (Slichter 1899).

2. Approximate solution of differential equations

As in a previous paper (Wooding 1957), the differential equations of slow steady flow may be expressed in dimensionless units. The temperature parameter θ is defined by

$$\theta = (T - T_0)/(T_1 - T_0), \tag{7}$$

where T_0, T_1 are two typical boundary temperatures. The 'equivalent flow' vector $\mathbf{q}_0$ is defined from the continuity relation

$$\rho\mathbf{q} = \rho_0\mathbf{q}_0, \tag{8}$$

in which it will be assumed that the density ρ of the liquid is related to the temperature by the approximate expression

$$\rho = \rho_0\{1 - \alpha(T_1 - T_0)\theta - \beta(T_1 - T_0)^2\theta^2\}, \tag{9}$$

ρ_0 being the density at temperature T_0, and α, β being constants. The modified Péclet number ζ is given by

$$(K_m/K_w)_0\,\zeta = \mathbf{q}_0\,d/\kappa_0, \tag{10}$$

where κ_0 is the thermal diffusivity of the liquid at temperature T_0, d is a typical length derived from the boundary dimensions, and $(K_m/K_w)_0$ is, as before, the ratio at T_0 of the thermal conductivity of the mixture to the thermal conductivity of the liquid.

Since the boundary conditions of the experiment have cylindrical symmetry, it is convenient to take axes in dimensionless units r, z, with Or horizontal and Oz directed vertically upwards, and to define Stokes' stream function ψ by

$$\boldsymbol{\zeta} = \mathbf{i}\psi_z/r - \mathbf{k}\psi_r/r, \tag{11}$$

$\mathbf{i}$, $\mathbf{k}$ being vectors in the directions Or, Oz respectively. The suffices in r, z signify partial differentiation.

Then, for slow steady motion of water in a saturated homogeneous permeable solid, the equations of energy and motion give in cylindrical

coordinates a pair of simultaneous partial differential equations for $\theta(r, z)$ and $\psi(r, z)$,

$$\theta_{rr}+\frac{1}{r}\theta_r+\theta_{zz}+b(T_1-T_0)\frac{1}{r}\{(r\theta\theta_r)_r+(r\theta\theta_z)_z\}=\frac{1}{r}(\psi_z\theta_r-\psi_r\theta_z)$$
$$=\frac{1}{r}\frac{\partial(\theta,\psi)}{\partial(r,z)}, \quad (12)$$

$$\psi_{rr}-\frac{1}{r}\psi_r+\psi_{zz}-\frac{a(T_1-T_0)}{1+a(T_1-T_0)\theta}(\theta_r\psi_r+\theta_z\psi_z)+$$
$$+\eta r\{1+a(T_1-T_0)\theta\}\{1+(2\beta/\alpha)(T_1-T_0)\theta\}\theta_r=0, \quad (13)$$

where
$$a=(T_0-260)^{-1}\,(^\circ\mathrm{A})^{-1} \quad (14)$$
is a temperature coefficient for viscosity.

For the approximate solution of equations (12) and (13) it will be assumed that η, b are small, and that θ and ψ may be expanded in power series involving these quantities. (Also, for convenience in later analysis, we introduce the notation $m=\eta/(T_1-T_0)$, the parameter m being independent of T_1-T_0.) Then the perturbation models will be written as

$$\theta=\theta_0+m(T_1-T_0)\theta_1+b(T_1-T_0)\theta^{(1)}+m^2(T_1-T_0)^2\theta_2+\ldots, \quad (15)$$
$$\psi=m(T_1-T_0)\psi_1+m^2(T_1-T_0)^2\psi_2+\ldots. \quad (16)$$

Here, the second-order term (in m^2) will be calculated in order to estimate the magnitude of the second-order correction. The second-order terms in mb, b^2 will be ignored, on the assumption that only the linear term in b has significance. The series solution (15) and (16) of the equations (12) and (13) may be fitted to suitable experimental data to obtain estimates of the parameters m and b.

Substitution of equations (15) and (16) into (12) and (13) gives a series of partial differential equations for the perturbation coefficients θ_0, ψ_1, θ_1, ψ_2, θ_2 and $\theta^{(1)}$,

$$(\theta_0)_{rr}+\frac{1}{r}(\theta_0)_r+(\theta_0)_{zz}=0, \quad (17)$$

$$(\psi_1)_{rr}-\frac{1}{r}(\psi_1)_r+(\psi_1)_{zz}-\gamma\{(\theta_0)_r(\psi_1)_r+(\theta_0)_z(\psi_1)_z\}+$$
$$+r\{1+a(T_1-T_0)\theta_0\}\{1+(2\beta/\alpha)(T_1-T_0)\theta_0\}(\theta_0)_r=0, \quad (18)$$

$$(\theta_1)_{rr}+\frac{1}{r}(\theta_1)_r+(\theta_1)_{zz}=\frac{1}{r}\frac{\partial(\theta_0,\psi_1)}{\partial(r,z)}, \quad (19)$$

$$(\psi_2)_{rr}-\frac{1}{r}(\psi_2)_r+(\psi_2)_{zz}-\gamma\{(\theta_0)_r(\psi_2)_r+(\theta_0)_z(\psi_2)_z\}-$$
$$-\gamma\{(\theta_1)_r(\psi_1)_r+(\theta_1)_z(\psi_1)_z\}+\gamma^2\theta_1\{(\theta_0)_r(\psi_1)_r+(\theta_0)_z(\psi_1)_z\}+$$
$$+r\{1+a(T_1-T_0)\theta_0\}\{1+(2\beta/\alpha)(T_1-T_0)\theta_0\}(\theta_1)_r+$$
$$+r[\{1+a(T_1-T_0)\theta_0\}(2\beta/\alpha)(T_1-T_0)\theta_1+$$
$$+\{1+(2\beta/\alpha)(T_1-T_0)\theta_0\}a(T_1-T_0)\theta_1](\theta_0)_r=0, \quad (20)$$

where $\gamma = a(T_1 - T_0)\{1 + a(T_1 - T_0)\theta_0\}^{-1}$,

$$(\theta_2)_{rr} + \frac{1}{r}(\theta_2)_r + (\theta_2)_{zz} = \frac{1}{r}\frac{\partial(\theta_0, \psi_2)}{\partial(r, z)} + \frac{1}{r}\frac{\partial(\theta_1, \psi_1)}{\partial(r, z)}, \tag{21}$$

$$\theta^{(1)}_{rr} + \frac{1}{r}\theta^{(1)}_r + \theta^{(1)}_{zz} + \{(\theta_0)^2_r + (\theta_0)^2_z\} = 0. \tag{22}$$

These are readily transformed into finite-difference equations by the usual procedures, taking a square mesh of element dimension h, and relaxation techniques may be applied in order to obtain approximate numerical solutions for the coefficients.

3. Description of apparatus and experimental procedure

Figure 1 illustrates in diagrammatic form the arrangement of temperature and flow boundaries chosen for the experimental work. Oz is the axis of two concentric cylinders AD, BC which have radii in the ratio 2:7. In

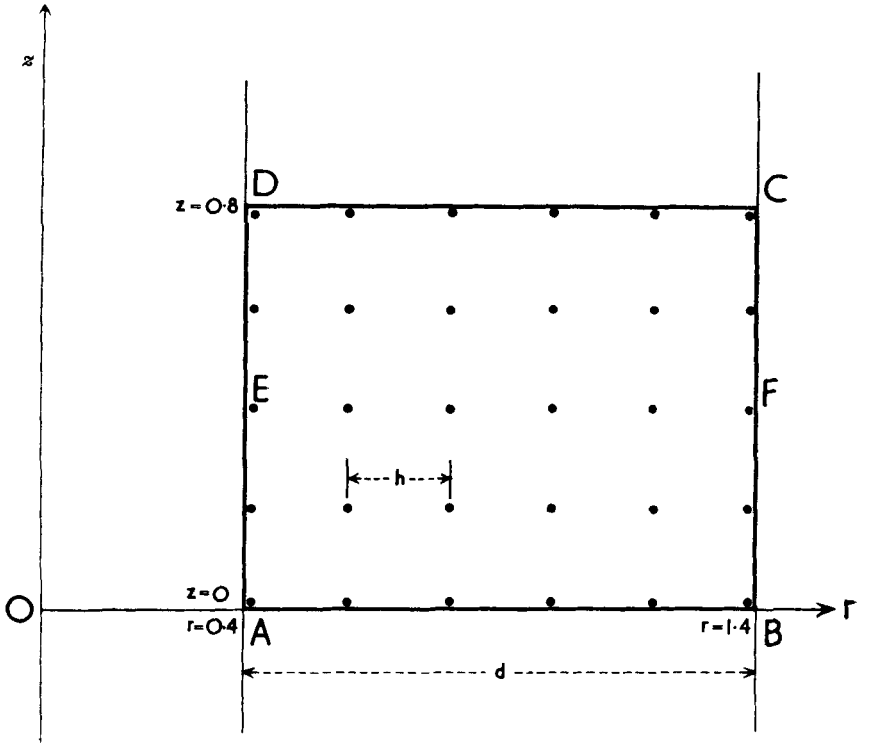

Figure 1. Boundary configuration of the cylindrical model, showing mesh points of the relaxation net.

the dimensionless system the length unit is taken as $d = AB$, giving the dimensionless r, z values shown for the various boundaries. The 30 points arranged in a square mesh represent points of the relaxation net, from which it will be seen that $h = \frac{1}{5}$ in dimensionless units. These points correspond to thermocouple positions in the experimental arrangement.

The cylinders AD and BC are held at constant temperatures T_1 and T_0 respectively ($T_1 > T_0$), while the boundaries AB, CD satisfy conditions of nearly complete thermal insulation. All four boundaries are impermeable to liquid. Consequently, the boundary conditions for the numerical calculations may be described ideally as follows:

$$\text{on } BC, \qquad \theta = 0;$$

$$\text{on } DA, \qquad \theta = 1;$$

$$\text{on } AB,\ CD, \qquad \theta_z = 0; \tag{23}$$

$$\text{on } AB,\ BC,\ CD,\ DA, \qquad \psi = 0. \tag{24}$$

A feature of these boundary conditions is that $(\theta_0)_z$ vanishes throughout equations (17) to (22).

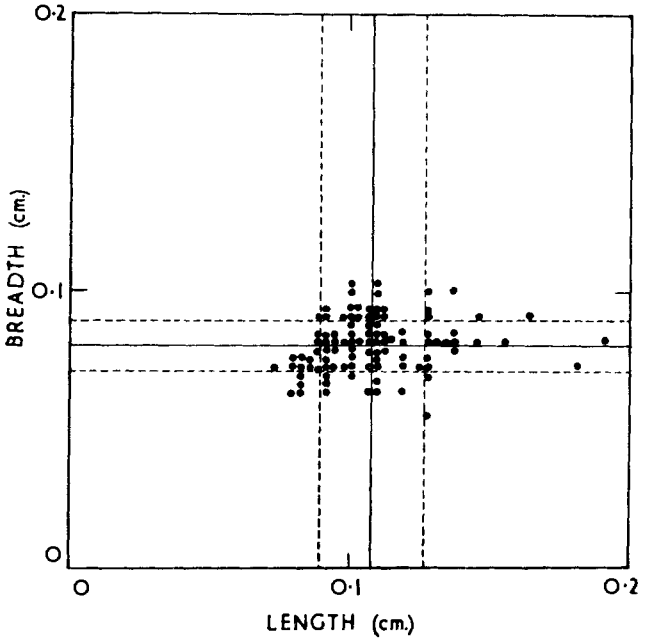

Figure 2. Length-breadth distribution of 100 grains of quartz sand. The regression lines and standard deviation have been calculated from a total sample of 233 grains.

In the experimental arrangement, two copper cylinders of radii 3·8 cm and 13·3 cm are arranged coaxially to represent boundaries DA and BC respectively. The outer cylinder is surrounded by a water jacket, while the inner cylinder forms the sides of a water-tight container. Constant, practically uniform, temperatures are maintained on the boundary cylinders by means of circulating water with thermostatic control.

The space between the temperature-controlled copper cylinders, of width $d = 9{\cdot}5$ cm, is filled with standard graded quartz sand (porosity 0·4

approximately) to a depth of $0{\cdot}8d$. Figure 2 is a scatter diagram showing the length–breadth relation for a sample of 100 sand grains, based on the assumption that each grain is approximately ellipsoidal. (Since these results have been obtained from a single photomicrograph, measurements are not available for the depth of each grain.) The sample is seen to be satisfactorily homogeneous, and if Δ is a typical dimension for grain size it follows that $\Delta/d = O(10^{-2})$.

A thin sheet of bakelite mounted vertically and radially supports copper–constantan thermocouples in the 30 positions shown in figure 1, the thermocouple leads being carried circumferentially for several centimetres from the junctions to reduce conduction errors. Each thermocouple junction is arranged to project about 0·4 cm beyond the bakelite sheet, and is supported by gluing the copper and constantan wires to the sheet For the thermocouples adjacent to the boundaries corresponding to BC and DA, extra support can be afforded by the cylinder walls, as these are in effective thermal contact with the thermocouples.

Although a boundary layer exists close to the vertical bakelite sheet, its effect upon the thermocouple readings can be considered negligible provided that $\delta \doteqdot \Delta \ll 0{\cdot}4$ cm, where δ is the thickness of the layer (§ 1). From figure 2 it appears that this condition is practically satisfied.

Thin sheets of bakelite sealed with a rubber-based glue render the upper and lower boundaries impermeable to moisture, and are backed by layers 3 cm thick of Perspex 'honeycomb' to provide thermal insulation. Compression applied to the top of the upper layer of insulating material is transmitted throughout the assembly, and ensures that (except for possible packing irregularities) the sand should have an approximately constant fluid permeability and thermal conductivity within the convection space.

After the convection space has been filled with boiled water, care being taken to exclude all air bubbles, the inner and outer boundaries are adjusted to have a suitable temperature difference which is maintained as nearly constant as possible. A period of up to four hours elapses before steady-state conditions are approached.

Three different values of the boundary temperature difference have been employed, the experimental average values of $T_1 - T_0$ being (I) 18·40° A, (II) 32·70° A, (III) 46·68° A. In each case, T_0 is held close to (273 + 20)° A, for which $\alpha = 2{\cdot}25 \times 10^{-4}$ (° A)$^{-1}$, $\beta = 3{\cdot}75 \times 10^{-6}$ (° A)$^{-2}$ in equation (9), and $a = 1/33$ (° A)$^{-1}$ in equation (14).

Experimental values θ_c of the convection temperature parameter are computed from the measured temperatures T (° A) using the formula (7). The results for the three experiments are given in table 1.

Steady-state conditions are found to be attainable on each cylindrical boundary to within $\pm 0{\cdot}05$° A for experiments I and II, and to within $\pm 0{\cdot}20$° A for experiment III. These results are obtained by observation of several boundary thermocouple outputs whilst the thermostats controlling the boundary temperatures pass through several 'on–off' cycles. It is easily shown from formula (7) that resultant variations in time of the

parameter θ_c are less than $\pm 0{\cdot}005$ for experiments I and II, and less than $\pm 0{\cdot}010$ for experiment III. Corresponding time variations in the interior thermocouples are much reduced, owing to the short period (five to eight minutes) of the boundary variations, which are lagged by the saturated sand.

Expt. I	*D* 999 (1)	686 (3)	472 (2)	275 (2)	119 (3)	*C* −7 (7)
	986 (14)	681 (4)	459 (2)	279 (1)	119 (1)	0 (0)
	E 1010 (−10)	673 (−1)	445 (0)	263 (0)	112 (0)	*F* 1 (−1)
	1004 (−4)	655 (−1)	416 (0)	243 (0)	100 (−1)	1 (−1)
	A 998 (2)	645 (0)	399 (0)	241 (0)	103 (−2)	*B* 6 (−6)
Expt. II	*D* 1003 (−3)	735 (0)	514 (0)	313 (1)	148 (2)	*C* −6 (6)
	997 (3)	710 (0)	486 (0)	305 (0)	141 (1)	−2 (2)
	E 1009 (−9)	680 (−2)	440 (−1)	263 (−1)	124 (−2)	*F* 7 (−7)
	999 (1)	613 (0)	387 (0)	224 (−1)	101 (−1)	−1 (1)
	A 993 (7)	587 (2)	353 (0)	210 (−1)	98 (−1)	*B* 2 (−2)
Expt. III	*D* 1020 (−20)	791 (−8)	593 (−4)	368 (−3)	189 (−3)	*C* 3 (−3)
	1008 (−8)	742 (−5)	533 (−3)	293 (−3)	166 (−3)	5 (−5)
	E 1009 (−9)	660 (−3)	437 (−1)	262 (−1)	123 (−2)	*F* 8 (−8)
	991 (9)	559 (4)	347 (2)	197 (2)	86 (3)	−7 (7)
	A 973 (27)	509 (10)	295 (4)	172 (3)	76 (5)	*B* −10 (10)

Table 1. Experimental values of the temperature parameter $10^3\theta_c$. Corresponding values of the boundary correction term $10^3\theta^{(0)}$ are shown in parentheses.

However, in the steady state, small spatial temperature variations occur in the Oz-direction along the boundaries DA and BC (table 1). These appear to be due to the finite effective conductivity of each cylindrical boundary system, emphasized perhaps by the presence of a steady flow pattern within the circulating water.

4. Analysis of results

As noted at the end of § 3, the steady-state values of θ_c obtaining on boundaries BC and DA vary by small amounts from the theoretical values of θ given by (23). The theoretical boundary conditions will now be fitted to the experimental values by applying a perturbation $\theta^{(0)}$ to θ, such that

$$\text{on } BC,\ DA,\ 1-\theta^{(0)} = \theta_c;$$
$$\text{on } AB,\ CD,\quad \theta_z^{(0)} = 0. \tag{25}$$

Also, let the definition of $\theta^{(0)}$ be such that

$$\theta - \theta^{(0)} = \theta_c \tag{26}$$

within the convection space. Here, θ can be assumed to be represented by the perturbation series (15). As $\theta^{(0)}$ is very small, cross-product terms

involving $m(T_1 - T_0)\theta_1\theta^{(0)}$, etc., will be neglected, whence it is readily shown that $\theta^{(0)}$ is harmonic to first order in the convection space. Values of $\theta^{(0)}$ calculated by relaxation methods are given in parentheses in table 1.

A further correction to the boundary conditions arises from the possibility of thermal radiation through the insulation at the boundaries AB, CD. Since the external ambient temperature is normally close to T_0, it is possible to assume that the radiation boundary conditions take the form

$$\text{on } CD,\ \theta_z = c\theta;$$
$$\text{on } AB,\ \theta_z = c'\theta. \tag{27}$$

With the assumption that the radiation constants c, c' are very small, it is possible to take first-order perturbations in θ of form

$$c\theta^{(2)} + c'\theta^{(3)}, \tag{28}$$

this expression being combined with (15).

$10^3\theta_0$	D	1000	677	447	269	123	C	0
$10^3\psi_1$	D	0	0	0	0	0	C	0
		0	−41	−52	−48	−32		0
	E	0	−51	−67	−62	−42	F	0
$10^4\theta_1$	D	0	131	136	96	47	C	0
		0	90	94	67	33		0
	E	0	0	0	0	0	F	0
$10^5\psi_2$	D	0	0	0	0	0	C	0
		0	8	−30	−46	−38		0
	E	0	0	0	0	0	F	0
$10^5\theta_2$	D	0	−25	2	17	13	C	0
		0	−27	−5	11	10		0
	E	0	−28	−11	5	7	F	0
$10^3\theta^{(1)}$	D	0	112	126	100	55	C	0
$10^3\theta^{(2)}$	D	0	144	146	105	52	C	0
		0	68	80	62	32		0
	E	0	35	45	37	20	F	0
		0	21	28	24	13		0
	A	0	17	23	20	11	B	0

Table 2. Numerical values of the perturbation coefficients calculated by relaxation methods for experiment I. The given values of θ_0, $\theta^{(1)}$ and $\theta^{(2)}$ apply for experiments I, II and III.

Tables 2, 3 and 4 give numerical values of the coefficients θ_0, ψ_1, θ_1, ψ_2, θ_2 and $\theta^{(1)}$, calculated by relaxation methods from equations (17) to (22) respectively, and using the boundary conditions derived by substitution of (15) into (23) and (16) into (24). Also tabulated are values of $\theta^{(2)}$, which are calculated from Laplace's equation with boundary conditions derived

by substituting (28) into (27). In all cases the relaxation net of figure 1 is used. In general, it is necessary to tabulate only part of the calculated field for each case, as both θ_0 and $\theta^{(1)}$ are constant with respect to z, while ψ_1 and θ_2 are symmetrical about the horizontal plane EF, and θ_1 and ψ_2

$10^3\psi_1$	D	0	0	0	0	0	C	0
		0	−59	−70	−60	−38		0
	E	0	−74	−91	−79	−50	F	0
$10^4\theta_1$	D	0	184	184	127	61	C	0
		0	126	127	88	43		0
	E	0	0	0	0	0	F	0
$10^5\psi_2$	D	0	0	0	0	0	C	0
		0	0	−77	−93	−65		0
	E	0	0	0	0	0	F	0
$10^5\theta_2$	D	0	−44	9	33	24	C	0
		0	−49	−4	22	19		0
	E	0	−53	−16	12	14	F	0

Table. 3. Numerical values of the perturbation coefficients calculated by relaxation methods for experiment II.

$10^3\psi_1$	D	0	0	0	0	0	C	0
		0	−80	−90	−74	−44		0
	E	0	−100	−117	−97	−58	F	0
$10^4\theta_1$	D	0	245	238	160	75	C	0
		0	167	164	111	52		0
	E	0	0	0	0	0	F	0
$10^5\psi_2$	D	0	0	0	0	0	C	0
		0	−22	−158	−165	−101		0
	E	0	0	0	0	0	F	0
$10^5\theta_2$	D	0	−70	23	58	39	C	0
		0	80	0	40	31		0
	E	0	−90	−22	23	23	F	0

Table 4. Numerical values of the perturbation coefficients calculated by relaxation methods for experiment III.

are antisymmetrical about EF. $\theta^{(2)}$ does not possess symmetry of this type, but $\theta^{(3)}$ and $\theta^{(2)}$ are related antisymmetrically about EF. Finally, the functions θ_0, $\theta^{(1)}$ and $\theta^{(2)}$ have the same values for experiments I, II and III.

Because of the small scale of the apparatus used, the sand grains are of appreciable size ($\Delta/d = O(10^{-2})$) and the spatial temperature gradient is

high, with resultant scatter in the experimental temperature readings. It is preferable, therefore, to use statistical methods (least squares) in fitting the theoretical model to the data of table 1 for the three values of the boundary temperature difference which are employed, and to use significance tests in evaluating the adequacy of the model.

Combination of equations (15) and (28) shows that the statistical temperature model will be of the form

$$\theta - \theta_0 = m(T_1 - T_0)\theta_1 + b(T_1 - T_0)\theta^{(1)} + c\theta^{(2)} + c'\theta^{(3)} + m^2(T_1 - T_0)^2\theta_2 + \epsilon, \quad (29)$$

to the order of accuracy considered, where all of the parameters m, b, c and c' should be constant for varying values of $T_1 - T_0$. Point values of the residual error variable ϵ will be assumed to be distributed approximately normally and independently of each other with zero mean. Since not all terms in the analysis are necessarily significant, and since the complete model would prove unwieldy when obtaining a least-squares fit, a series of partial models will be used, each model involving not more than three of the parameters on the right-hand side of (29). For future reference, each partial model will be labelled H_i, with residual variable ϵ_i and a corresponding suffix will be used to identify the parameters retained.

Table 5 gives the numerical results obtained with a number of partial models for the three cases I, II and III by the usual least-squares methods. In table 5, entries from the left are in terms of model number i, parameters retained in model i, degrees of freedom ν_i, experiment number (I, II or III), optimal parametric estimates, and standard error of estimates. The significance of each added parameter is estimated by means of the variance ratio F_{ij}, computed from the residual sums of squares $\sum(\epsilon_i^2)$, $\sum(\epsilon_j^2)$ for the ith and jth models respectively ($i > j$), from the formula

$$F_{ij} = F(Q_F|\nu_j - \nu_i, \nu_j) = \frac{\{\sum(\epsilon_j^2) - \sum(\epsilon_i^2)\}/(\nu_j - \nu_i)}{\sum(\epsilon_i^2)/\nu_i}, \quad (30)$$

(Pearson & Hartley 1954). Each tabulated value of Q_F gives the probability of exceeding the observed F-ratio by chance. Thus, a very small value of Q_F implies that the added parameter is significant.

The models H_1, H_2 and H_3, ($i = 1, 2, 3$ in table 5), are intended to test the significance of the convection effect to first and second orders respectively. However, H_3 cannot be tested against H_2 by the usual significance tests, since m, m^2 are not independent parameters. A conservative test for *non*-significance of m^2 may be obtained by replacing m^2 with an independent parameter l (H_4), and testing H_4 against H_2. Thus, if this test shows that the effect of l is non-significant, then the effect of m^2 will be non-significant also.

Values of the parametric estimates $\hat{m}_2 = \hat{\eta}_2/(T_1 - T_0)$, $\hat{c}_5$, $\hat{b}_6$ from table 5 are plotted in figure 3 (*a*), (*b*) and (*c*) respectively, these being chosen since they represent values estimated from the simplest models.

i	Parameters retained	ν_i	Expt.	Parametric estimates	Standard errors of estimates	F_{ij}	Q_F
1	—	20	I	—	—	—	—
			II	—	—	—	—
			III	—	—	—	—
2	m	19	I	$\hat{m} = 0{\cdot}118$ (° A)$^{-1}$	0·016 (° A)$^{-1}$	$F_{21} = 57$	$\ll 10^{-3}$
			II	0·126	0·006	255	
			III	0·120	0·006	410	
3	m, m^2	19	I	—	—	—	—
			II	—	—	—	—
			III	—	—	—	—
4	m, l	18	I	—	—	$F_{42} = 0$	N.S.*
			II	—	—	2	N.S.
			III	—	—	6	$\leqslant 0{\cdot}025$
5	m, c	18	I	$\hat{c} = -0{\cdot}16$	0·03	$F_{52} = 35$	$< 10^{-3}$
			II	−0·16	0·02	50	$< 10^{-3}$
			III	−0·17	0·07	7	$\leqslant 0{\cdot}025$
6	m, b	18	I	$\hat{b} = -0{\cdot}0046$ (° A)$^{-1}$	0·0008 (° A)$^{-1}$	$F_{62} = 37$	$< 10^{-3}$
			II	−0·0025	0·0004	61	$< 10^{-3}$
			III	−0·0023	0·0007	11	$< 0{\cdot}025$
7	m, c, b	17	I	—	—	$F_{76} = 0$	N.S.
			II	—	—	2	N.S.
			III	—	—	1	N.S.

(* N.S. = not significant.)

Table 5. Statistical results obtained by fitting perturbation models to the separate groups of experimental data I, II and III.

Also shown in figure 3 are overall estimates $\hat{m}_2'$, $\hat{c}_5'$, $\hat{b}_6'$, which are obtained by assuming the hypothesis that the quantities m, c, b are constant for experiments I, II and III, and obtaining least-squares estimates using the combined data. These results are summarized in table 6, and are distinguished from the results of table 5 by dashes. The variance ratio F_{ij}'

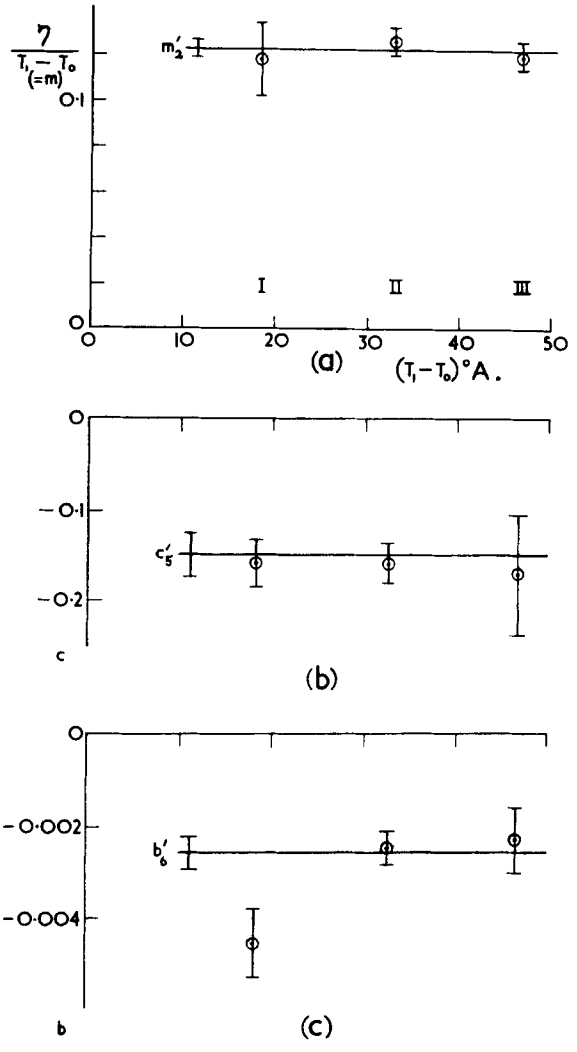

Figure 3. Values of the parametric estimates from table 5 for experiments I, II and III, and the overall estimates from table 6 for (*a*) m_2, (*b*) c_5, (*c*) b_6.

is used to examine the significance of the effect of each added parameter m_i', b_i', c_i', and the variance ratio F_{ii}' is used to examine the significance of the increase in the residual sum of squares $\sum(\epsilon_i'^2)$ over the sum of the three individual sums of squares $\sum(\epsilon_i^2)$ given for the ith model in table 5.

i, i'	Parameters retained	ν_i'	$\sum_3 \nu_i^*$	Parametric estimates	Standard errors of estimates	F_{ij}'	Q_F'	F_{ii}'	Q_F
1	—	60	60	—	—	—	—	—	—
2	m	59	57	$\hat{m} = 0{\cdot}122\,(^\circ\,\mathrm{A})^{-1}$	$0{\cdot}004\,(^\circ\,\mathrm{A})^{-1}$	$F_{21}' > 1000$	$\ll 10^{-3}$	$F_{22}' = 0$	N.S.
5	m, c	58	54	$\hat{m} = 0{\cdot}121$ $\hat{c} = -0{\cdot}15$	$0{\cdot}003$ $0{\cdot}02$	$F_{52}' = 38$	$\ll 10^{-3}$	$F_{55}' = 1$	N.S.
6	m, b	58	54	$\hat{m} = 0{\cdot}122$ $\hat{b} = -0{\cdot}0026\,(^\circ\,\mathrm{A})^{-1}$	$0{\cdot}003$ $0{\cdot}0004\,(^\circ\,\mathrm{A})^{-1}$	$F_{62}' = 52$	$\ll 10^{-3}$	$F_{66}' = 0$	N.S.
6*a*	m, m^2, b	58	54	$\hat{m} = 0{\cdot}119$ $\hat{b} = -0{\cdot}0023$	— —	— —	— —	— —	— —
7	m, b, c	57	51	$\hat{m} = 0{\cdot}124$ $\hat{c} = -0{\cdot}03$ $\hat{b} = -0{\cdot}0021$	$0{\cdot}004$ $0{\cdot}04$ $0{\cdot}0007$	$F_{75}' = 9$ $F_{76}' = 1$	$\ll 0{\cdot}005$ N.S.	$F_{77}' = 1$	N.S.

($^* \sum_3 \nu_i$ = sum of degrees of freedom for I, II and III from table 5.)

Table 6. Statistical results obtained by fitting perturbation models to the combined data of experiments I, II and III.

5. Discussion of statistical results

In table 5 for $i = 1, 2$, the values of F_{21} show that the parameter $m = \eta/(T_1 - T_0)$ in the first-order model has a very high significance, which increases with $(T_1 - T_0)$ as the convection effect becomes increasingly dominant over secondary effects. Hence the null hypothesis $H_1(\theta - \theta_0 = \epsilon_1)$ must be rejected, and the presence of a convection phenomenon appears to be well established. However, from F_{42} the effect of the second-order term (m^2) is not significant in experiments I and II, and the effect in III is probably not significant. Presumably, the term in m^2 would become significant for larger values of $(T_1 - T_0)$ than are available in these experimental data.

Separate tests of the effects of the parameters m, c and m, b against m (F_{52}, F_{62} respectively) show comparable significance for the reduction in residual sums of squares in the two cases. However, with the effect of m, c, b tested against m, b (F_{76}), there is not a significant reduction in residual sum of squares. It appears that this result is due to the similarity, analogous to a high correlation, between the coefficients of c and b. In physical terms, the effect of radiation through the upper insulated boundary (coefficient c) is very similar in form to the effect of variation in thermal conductivity due to the negative temperature coefficient (b) of the quartz sand. Both phenomena tend to reduce the temperature within the convection field, and since each effect is small, the present method of analysis is not able to resolve them completely.

An additional test, of the parameters m, c, c' against m, c, shows that c' has no significance. It follows that radiation through the lower boundary surface is negligible.

To examine the significance of the dispersion term (§ 1), a further test is formulated using m, b, c and an additional perturbation parameter representing the effect of simple isotropic dispersion. As the three values obtained for the coefficient of the additional parameter are scattered closely about zero, it can be concluded that there is negligible dispersion of heat by irregularities of the fluid motion.

Considerable heterogeneity of residual variance $\sum(\epsilon_i^2/\nu_i)$ has been found between the results of experiments I, II and III, much of the heterogeneity being due to a relatively large residual variance in III. Physically, it would appear that the higher temperatures involved in III have resulted in poorer stabilization, the residual standard error in the temperature measurements being given by (I) $\pm 0{\cdot}12°$ A, (II) $\pm 0{\cdot}18°$ A, (III) $\pm 0{\cdot}69°$ A respectively, after m, b and c have been fitted. These values are larger than the time variations mentioned in § 3, since steady-state scatter in the thermocouple readings is present also. The effect of this heterogeneity of variance is to modify the distribution of the F'-values given in table 6 and the corresponding values of Q'_F may therefore be only an indication of the true values. Although it follows that the results of table 6 are statistically less reliable than the results of table 5, the Q'_F-values in table 6 are all either so large or so small that any numerical modification necessary is unlikely to alter their physical implications.

The results of the overall tests F'_{22}, F'_{55}, F'_{66}, F'_{77} (table 6) show that the hypothesis that m, b, c are constant is not disproved. The standard error of the estimate $\hat{m}'_2$ is about $\pm 3\%$. Constant values of these three parameters are expected, of course, since none is dependent upon $(T_1 - T_0)$, the quantity varied between the three experiments.

It will be seen that the test F'_{76} (which tests m, b, c against m, b) does not give significance. If the simpler model is desired, therefore, one could ignore boundary radiation and choose the model H'_6 in preference to H'_7.

A further hypothesis H'_{6a}, using the overall data to fit m to second order and b to first order as in equation (15), is found to give the same residual sum of squares as H'_6. Hence there is no preference for or against the second-order model when it is compared with the first-order model.

6. Supplementary observations and results

In order to calculate an approximate value for m by alternative means, it is necessary to measure the permeability of quartz sand under compression conditions resembling those of the convection experiment, and to measure the thermal conductivity of quartz sand at temperature T_0 in the absence of convection. A standard permeability experiment of Darcy type (Muskat 1937) has been set up, the sand being carefully tapped down and compressed as in the convection model, and a value of

$$k = (2{\cdot}61 \pm 0{\cdot}05) \times 10^{-6} \text{ cm}^2 \tag{31}$$

has been obtained. For the conductivity measurement, water-saturated quartz sand is compressed between a pair of square horizontal plates, the upper plate being at the higher temperature. A conductivity value of

$$(K_m)_0 = (4{\cdot}60 \pm 0{\cdot}05) \times 10^{-3} \text{ c.g.s. units} \tag{32}$$

has been obtained at $(20 + 273)^\circ$ A. With these values for k and $(K_m)_0$, and with $\alpha = 2{\cdot}25 \times 10^{-4} (^\circ\text{A})^{-1}$, $d = 9{\cdot}5$ cm, $g = 980$ cm sec^{-2}, $\nu_0 = 0{\cdot}010$ cm^2 sec^{-1} units, equation (2) gives

$$m = \eta/(T_1 - T_0) = 0{\cdot}119 \pm 0{\cdot}003\,(^\circ\text{A})^{-1}. \tag{33}$$

This value is in very good agreement with the least-squares estimates of m in § 4, table 6. It will be seen that m has been determined with approximately the same standard error by either method.

From these values of m, it is a simple calculation to show that the ratio

$$(K_m/K_w)_0(\kappa_0 \nu_0/k) = 17{\cdot}5 \pm 0{\cdot}5 \text{ cm}^2 \text{ sec}^{-2} \tag{34}$$

for $T_0 = (273 + 20)^\circ$ A and for the particular water-saturated quartz sand used in the experimental work. This result, which is a property of the sand and water alone, is of more general usefulness than m, as it is independent of the boundary conditions used in the model.

A rough estimate of b has been obtained from the data on thermal conductivity of quartz published in the International Critical Tables

(National Research Council, U.S.A. 1929). In the temperature range 20° C to 70° C, the thermal conductivity of quartz can be represented approximately by

$$K_s = 0{\cdot}029\{1 - 0{\cdot}0037(T - T_0)\} \text{ c.g.s. units}$$

parallel to the principal axis of the crystal, and

$$K_s = 0{\cdot}016\{1 - 0{\cdot}0024(T - T_0)\} \text{ c.g.s. units}$$

perpendicular to the principal axis, where $T_0 = (273 + 20)°\,\text{A}$. If the directions of the principal axes of the sand grains can be assumed to have a spherical distribution, and if the quartz contributes the major share of the thermal conductivity, the average value of the temperature coefficient would be approximately

$$b = -0{\cdot}0028(°\,\text{A})^{-1}. \tag{35}$$

This is to the same order as the values of b estimated in § 4, table 6.

r (non-dimensional)	0·6	0·8	1·0	1·2
$q \times 10^4$ (cals cm^{-2} sec^{-1})	5 ± 2	5 ± 2	3 ± 2	3 ± 2

Table 7. Measurement of flux of heat output through upper insulation.

An independent estimate of c can be obtained from the approximate formula

$$\frac{2\pi d}{(K_m)_0(T_1 - T_0)} \int_{0{\cdot}4}^{1{\cdot}4} qr\, dr = -2\pi c \int_{0{\cdot}4}^{1{\cdot}4} \theta_z^{(2)} r\, dr, \tag{36}$$

where q is the outflux of heat per unit area in c.g.s. units, and $\theta^{(2)}$ is the coefficient of c in the perturbation formulae. To measure q, a series of four differential thermocouples (calibrated as heat flux meters) are placed on the upper insulation at radii r corresponding to points of the relaxation net. The results are given in table 7, using the boundary conditions as for experiment I. After the integrals in (36) have been evaluated approximately, a value of

$$c = -0{\cdot}10 \pm 0{\cdot}05 \tag{37}$$

is obtained. This result is to the same order as the values of c estimated in § 4, table 6.

7. Conclusions

Evidently the first-order perturbation scheme provides a satisfactory fit to the convection data for the range of boundary temperature differences $(T_1 - T_0)$ chosen. Its range of validity extends from $\eta = m(T_1 - T_0) = 0$ to the point where the second-order term becomes significant in comparison with the term of first order. Presumably terms of higher order can be calculated, with increasing computational difficulty, but accuracy is not easily maintained owing to cumulative errors.

With the above limitation to first-order accuracy, it appears that the following additional conclusions have been justified experimentally.

(*a*) The motion of the liquid percolating through the sand under non-isothermal conditions is adequately described by Darcy's law for the low values of Reynolds number ($\ll 1$) applying here.

(*b*) The hypothesis that the packed sand behaves as an approximately homogeneous permeable medium is satisfactory.

(*c*) Near a fixed impermeable boundary, changes in sand packing due to the presence of a rigid surface might be expected to produce a thin layer of altered permeability. Neglect of this effect does not appear to introduce detectable errors: hence it is not of importance.

(*d*) Modifications to the apparent thermal conductivity at very low Reynolds numbers by fluid dispersion (§ 1) is negligible.

(*e*) The thickness of the fluid boundary layer adjacent to smooth rigid boundaries is small, probably close to the typical grain size.

The conditions (*a*) to (*e*) represent initial assumptions which are contained implicitly in the theoretical solutions. Departures from these conditions are negligible in comparison with the convection and other effects analysed above, since the residual variance after fitting m, b, c is very small.

While the analysis of thermal boundary loss and variation of thermal conductivity with temperature does not give accurate results, it is clear that these effects are small when compared with the convection effect. The estimate of m is not altered appreciably by their presence, and the general conclusions about the convection process are not affected.

The author wishes to thank the Director, Dominion Physical Laboratory, New Zealand Department of Scientific and Industrial Research, for making experimental facilities available, and Mr R. F. Benseman who was closely associated with the author in carrying out the experimental work. Thanks are due also to Dr J. H. Darwin and Mr A. McNabb of Applied Mathematics Laboratory for helpful suggestions, and to Mrs J. B. Wooding, who performed many of the numerical computations required in the analysis of the results.

References

Batchelor, G. K. 1954 *Quart. Appl. Math.* **12**, 209.

Chandrasekhar, S. 1943 *Rev. Mod. Phys.* **15**, 1.

Muskat, M. 1937 *The Flow of Homogeneous Fluids Through Porous Media.* Ann Arbor: Edwards.

National Research Council, U.S.A. 1929 *International Critical Tables*, Vol. 4. New York: McGraw-Hill.

Pearson, H. S. & Hartley, H. O. 1954 *Biometrika Tables for Statisticians*, Vol. 1. Cambridge University Press.

Rayleigh, Lord 1899 *Phil. Mag.* **47**, 246.

Slichter, C. S. 1899 *United States Geological Survey*, 19th annual report, part **2**, p. 295.

Wooding, R. A. 1957 *J. Fluid Mech.* **2**, 273.